Chemical Engineering Journal 326 (2017) 477–488

Contents lists available at ScienceDirect

Chemical Engineering Journal

journal homepage: www.elsevier.com/locate/cej

CO_2 dissociation in a packed bed DBD reactor: First steps towards a better understanding of plasma catalysis

I. Michielsen [a,*], Y. Uytdenhouwen [a], J. Pype [a,b], B. Michielsen [b], J. Mertens [c], F. Reniers [c], V. Meynen [a,b], A. Bogaerts [a]

[a] Department of Chemistry, University of Antwerp, Universiteitsplein 1, Wilrijk B-2610, Belgium
[b] Flemish Institute for Technological Research (VITO), Boeretang 200, Mol B-2400, Belgium
[c] Analytical and Interfacial Chemistry (CHANI), Faculty of Sciences, Université Libre de Bruxelles, Boulevard du Triomphe 2, Bruxelles B-1050, Belgium

HIGHLIGHTS

- The impact of the packing (support) material itself cannot be neglected.
- There is a large effect of the reactor setup and reactor/bead configuration.
- Comparing results obtained in different reactor setups should be done with care.
- $BaTiO_3$ yields the best results, i.e. 25% (conversion) and 4.5% (energy efficiency).

ARTICLE INFO

Article history:
Received 25 February 2017
Received in revised form 30 May 2017
Accepted 30 May 2017
Available online 1 June 2017

Keywords:
CO_2 dissociation
Dielectric barrier discharge reactor
Plasma catalysis
Reactor configuration
Shaped packing materials/supports

ABSTRACT

Plasma catalysis is gaining increasing interest for CO_2 conversion, but the interaction between the plasma and catalyst is still poorly understood. This is caused by limited systematic materials research, since most works combine a plasma with commercial supported catalysts and packings. In the present paper, we study the influence of specific material and reactor properties, as well as reactor/bead configuration, on the conversion and energy efficiency of CO_2 dissociation in a packed bed dielectric barrier discharge (DBD) reactor. Of the various packing materials investigated, $BaTiO_3$ yields the highest conversion and energy efficiency, i.e., 25% and 4.5%.

Our results show that, when evaluating the influence of catalysts, the impact of the packing (support) material itself cannot be neglected, since it can largely affect the conversion and energy efficiency. This shows the large potential for further improvement of packed bed plasma reactors for CO_2 conversion and other chemical conversion reactions by adjusting both packing (support) properties and catalytically active sites. Moreover, we clearly prove that comparison of results obtained in different reactor setups should be done with care, since there is a large effect of the reactor setup and reactor/bead configuration.

1. Introduction

1.1. General introduction

Carbon dioxide (CO_2), one of the major contributors to the greenhouse gas effect, exhibits an increasing concentration in the atmosphere. To reduce this concentration and the effect of CO_2 on global warming [1–4], a lot of technologies/reactions are considered, like (dry) reforming of methane for syngas production, CO_2 hydrogenation for the synthesis of methanol, methane, formaldehyde, dimethyl ether, etc [5,6]. However, CO_2 can also be directly split into CO and O_2, where CO can be used as a chemical feedstock for the production of value-added chemicals [7].

Abbreviations: SI, supporting information; DBD, dielectric barrier discharge; Q, charge; U, voltage; HV, high voltage; GC, gas chromatograph; RT-Q, 100% divinylbenzene column; RTX-f, fused silica column; $CO_{2,in}$, amount of CO_2 measured with the GC, without plasma; $CO_{2,out}$, amount of CO_2 measured with the GC, with plasma; X_{CO2}, the conversion of CO_2; X_{Real}, the actual conversion, corrected for the gas expansion; X_{GC}, the conversion matched to the one measured by the GC; ΔH_R, the reaction enthalpy of CO_2 dissociation (i.e., 279.8 kJ/mol); SEI, specific energy input in the plasma; η, energy efficiency; NH_3-TPD, ammonia temperature programmed desorption; TCD, thermal conductivity detector; FID, flame ionisation detector; ε, dielectric constant; TGA, thermogravimetric analysis.

* Corresponding author.
E-mail address: inne.michielsen@uantwerpen.be (I. Michielsen).

http://dx.doi.org/10.1016/j.cej.2017.05.177
1385-8947/

Since CO_2 has a high thermodynamic stability, a large amount of energy is needed to activate the CO_2 gas. When aiming for a thermal activation, a lot of energy (typically a temperature of more than 1500 K [8]) is lost in heating the entire gas. This inefficient conversion of CO_2 can be tackled by using non-thermal plasma technology, which provides an attractive alternative to the conventional (catalytic) thermal route [9–13], because of its possibility to accommodate chemical reactions close to room temperature in a non-equilibrium, low-energy-consuming reactor [14,15]. Indeed, a non-thermal plasma is characterized by a low overall gas kinetic temperature, while the electrons are accelerated by the applied electric field, and have typical energies of 1–10 eV, enough to break most chemical bonds (the standard reaction enthalpy for CO_2 dissociation is 2.9 eV).

Up till now, several types of plasma reactors have been investigated for CO_2 conversion, including corona discharges, glow discharges, microwave discharges, radio frequency discharges, gliding arc discharges and dielectric barrier discharges [16–26]. In this work, a dielectric barrier discharge (DBD) reactor is used, since it operates at ambient temperature and atmospheric pressure, can easily accommodate packing materials and be scaled up to industrial conditions [27].

1.2. State of the art

Despite great efforts in research towards an energy efficient conversion of CO_2 in an empty DBD reactor, the highest value obtained so far for CO_2 dissociation in CO and O_2 is 34% conversion, with 2% energy efficiency [28]. These values were obtained at 40 W plasma power, a frequency of 23.5 kHz and a discharge gap of 1.8 mm. By altering the conditions (lower SEI), the energy efficiency can reach 9%, but this corresponds to a drop in the conversion to only 8% [28].

To improve the energy efficiency of CO_2 dissociation in a DBD plasma, and to enhance the product selectivity in mixtures of CO_2 with a H-source gas, like CH_4, H_2O or H_2, a catalytic material can be added to the plasma reactor [5,29–31]. Plasma catalysis, where a plasma and a catalyst are combined, is very promising for environmental applications, and often leads to a synergy in terms of energy efficiency, product selectivity and yield, compared to merely plasma or catalysis [32]. For instance, it was demonstrated for pure CO_2 dissociation that the introduction of a dielectric packing into a DBD plasma reactor can enhance both the CO_2 conversion and energy efficiency up to a factor 1.9 and 2.2, respectively, compared to an unpacked DBD reactor [33–35]. Another study suggests that the conversion and energy efficiency double for the dry reforming of methane when adding a Ni/Al_2O_3 catalyst. Indeed, introducing a packing into a DBD can have multiple effects on the conversion and energy efficiency, by enhancing the electric field, changing the discharge type, altering the reactant concentration, etc [36].

Other studies on CO_2 dissociation were performed in packed bed DBD reactors with Ni, Ag or Pd catalysts, coated on an Al_2O_3 support [15,37–39], quartz wool, or zeolite 3A [40]. Comparison between the various experiments, in order to draw conclusions, is not straightforward, because of the difference in physical appearance between quartz wool, Al_2O_3 pellets of 500–850 μm and zeolite 3A beads of 2 mm, and thus, the effect is most likely not only correlated to one parameter (or one reactor configuration). In other papers [41,42], only 1 type of support was studied, therefore only investigating the enhancement of adding a catalytic element and neglecting the effect of the support.

The possible synergy between plasma and catalyst is not only dependent on the material of the packing/catalyst, but can also be based on changes of the plasma characteristics due to the presence of the packing. Therefore, a possible positive or negative effect depends on the change in discharge type, electric field, sorption effects, changes in the produced plasma species, etc [15]. Based on modelling, the physical effect of inserting a packing has been attributed to the contact between different beads inside the plasma reactor and between the beads and the dielectric barrier [33]. Indeed, the applied potential difference between the electrodes of the DBD reactor causes polarization of the (typically) dielectric beads, creating a strong electric field near the contact points [43]. This enhanced electric field strength is stated to be, at least partly, responsible for the higher conversion and energy efficiency [44]. According to previous work, quartz wool also improves the conversion of plasma-based dry reforming in a DBD with two quartz dielectric barriers [40], and enhances the conversion of methane and the yield of H_2 due to the physical properties of the discharge. A higher intensity of microdischarge filaments [40] and a change in discharge type from microdischarges to surface discharges on the quartz wool have been reported as reasons for these improved conversions [14].

Another important characteristic, as demonstrated by Van Laer and Bogaerts (both through modelling and experiments for a ZrO_2 packing), is the catalyst/packing size. Packing beads should have a diameter of at least 1/3 of the gap size to enhance the conversion and energy efficiency of CO_2 dissociation [33], with even a possible negative effect of very small beads, since the packing lowers the residence time. When the latter effect is larger than the positive electric field enhancement effect, it will eventually reduce the conversion [35].

Previous work also reported that adding a packing inside the gap reduces the available discharge volume, which limits the possible trajectory of the filamentary microdischarges. Therefore, only weak filaments can be generated in the voids between beads and between beads and a dielectric barrier, which has a negative effect on the conversion and energy efficiency, as was demonstrated for a Ni/Al_2O_3 packing material. The determining factor for the generation of these filaments is stated to be the distance between the beads or the beads and the dielectric barrier [15].

Next to the material of the catalyst/packing and the bead and gap size, also the material properties of the dielectric barrier affect the interaction between the beads and the dielectric. The influence of the dielectric barrier material itself [45], being the reactor tube, was demonstrated for $Ca_{0.7}Sr_{0.3}TiO_3$ with 0.5 wt% $Li_2Si_2O_5$, Al_2O_3 and silica glass (SiO_2), where the CO_2 conversion was reported to decrease in this order. However, this research was performed for an empty (i.e., non-packed) DBD, so no interaction with a packing could be studied here [46,47].

Moreover, various reports indicate that the conversion and energy efficiency also depend on the morphology, dielectric properties and chemical activity (e.g. acid-base properties) of the packing material, which was seen by Yu et al. [48] and Duan et al [49] in their studies of CO_2 decomposition on materials such as quartz, alumina, CaO and MgO. Other materials have been studied as well, like $BaTiO_3$ and ZrO_2, which have been found to improve the conversion and energy efficiency in a packed bed DBD reactor for CO_2 dissociation. However, these experiments were performed for only one dielectric barrier material [48,49]. Therefore, they cannot be simply combined in a general conclusion towards the effect of dielectric packing and dielectric barrier material for the dissociation of CO_2.

1.3. Aim of this work

Although several experimental studies have been performed to better understand and optimize plasma catalysis, as outlined above, the interactions between the plasma and the catalyst/packing are still poorly understood [15,37–42,50–53]. The most important element that is limiting this understanding and further progress

is the fact that no distinction can be made between the chemical and physical effects that may cause the synergy between plasma and catalyst. Most works combine a plasma with a commercial catalyst, being a catalytic active element deposited on a support and sometimes also containing binders and promoters [31,37–42,51,54–62].

In the present study, we thus investigate the influence of specific packing material (without catalytic activation, although we cannot exclude intrinsic catalytic activity of the support material itself) and reactor properties, as well as reactor/bead configuration, on the conversion and energy efficiency of CO_2 dissociation in a packed bed DBD reactor. More specifically, we focus our study on the interaction between (different types of) dielectric barriers (for different materials) and the physicochemical packing properties (size and chemical composition of the packing beads), and the ratio between the bead size and the gap size of the reactor.

The packing materials will consist of glass wool, quartz wool and spherical beads of SiO_2, ZrO_2, Al_2O_3 and $BaTiO_3$ with different controlled sizes. The dielectric barrier material consists of quartz and alumina. Although we cannot study all material combinations, a selection has been made based on diverging material properties with an initial focus on dielectric constant, and valuable insights in these combined effects are revealed.

2. Materials and methods

2.1. Setup of the packed bed DBD reactor

To study the influence of a dielectric packing in a packed bed DBD reactor, we apply the setup illustrated in Fig. 1. Various spherical dielectric beads are inserted, differing in composition and bead size (summarised in Table 1). To economize on beads, only the plasma zone (length of the outer electrode, 10 cm) is filled with beads, and glass wool is placed at both sides just outside of the plasma zone to prevent the beads from moving.

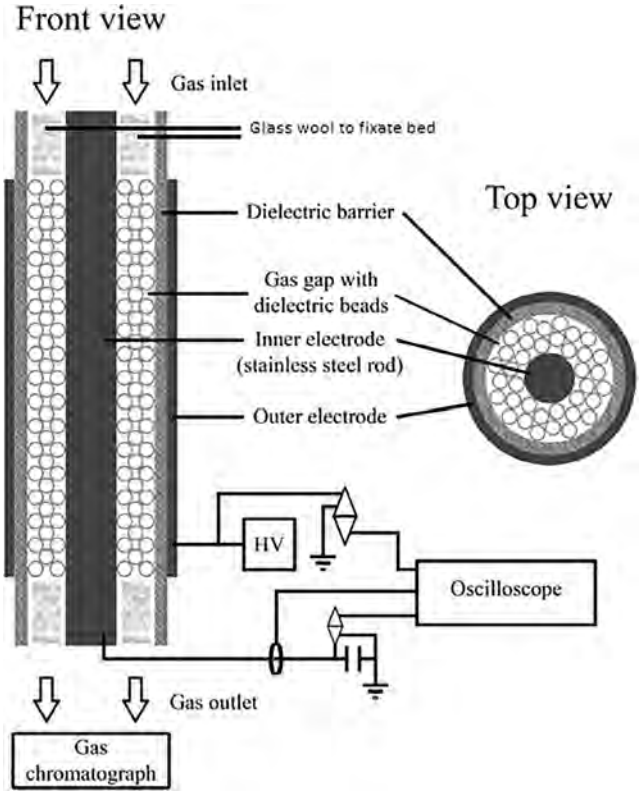

Fig. 1. Setup of the packed bed DBD reactor used in this study (adapted from Ref. [33]). The packing is illustrated with beads but can also be filled with glass wool or quartz wool.

The material of the dielectric barrier and the gap size are varied as well, as summarized in Table 1. In this way, we can study the influence of the interaction between the dielectric barrier (material properties and gap size) and packing properties (size and composition). For further comparison with literature, we also perform an experiment to study the influence of quartz wool and glass wool in the reactor.

A stainless steel rod is used as the inner electrode, with an outer diameter of 8, 10, 12 or 13 mm. A dielectric barrier (tubular reactor) is placed around the inner electrode, consisting of either alumina or quartz. Its inner diameter is 17 mm in both cases, resulting in a gas gap of 4.5, 3.5, 2.5 or 2 mm. Its outer diameter is 21.8 mm, corresponding to a barrier thickness of 2.4 mm. A stainless steel outer electrode is placed around the dielectric barrier.

The inner electrode is grounded, while the outer electrode is powered by a high voltage, supplied by a generator and transformer (AFS GmbH, Germany). The applied voltage is measured with a high voltage probe (Tek P6015A), while a Rogowski coil (Pearson 4100) is used to measure the total current. Moreover, the voltage is measured on an external capacitor (10 nF) to obtain the generated charges (Q) in the plasma. Plotting Q as a function of the applied voltage (U) gives us a Q-U Lissajous plot, characterizing the electrical properties in the plasma (See Fig. SI 2). Finally, all electrical signals are recorded by an oscilloscope (PicoScope 6402 A).

The temperature inside the reactor cannot be measured in our setup, as it would affect the plasma performance, but IR measurements of the dielectric barrier and the outer electrode were taken. An example is added to the supporting information, and is representative for all sizes and materials tested. The temperature obtained from these measurements is in the order of 419 K, but of course it only provides information for the outer electrode and dielectric barrier. We did not observe a correlation between the results obtained and the temperatures measured.

The input gas flow of CO_2 is controlled by thermal mass flow controllers (Bronkhorst) and the gas at the outlet is analysed by an online gas chromatograph (Trace GC 1310, Interscience). The GC is equipped with a thermal conductivity detector and a flame ionisation detector, and 4 columns: a Molsieve 5A, 2 RT-Q bonds and an RTX-f column. For the current application, the components were split with the Molsieve 5A and the 2 RT-Q bond-columns, and detected with the TCD. All measurements for the same conditions are repeated three times (to account for the influence of repacking the reactor), and every measurement includes 4 GC and power measurements, to obtain a standard deviation based on 12 measurements of the same condition. Care was taken to pack the reactor reproducibly, with an extra vibrating step, to ensure a dense packing. As can be seen in some sections, certain results will display large error bars. When this was the case, a Dixon Q test was performed, and no outliers could be rejected. The larger error bars were not material nor parameter dependent, which is why this large uncertainty cannot be explained nor prevented yet.

First, blank measurements of the amount of CO_2 are taken, i.e., without plasma. The amount of CO_2 measured here, is defined as $CO_{2,in}$. Subsequently, a power of 100 W is applied, with a frequency of 23.5 kHz, and after 40 minutes, i.e. when the measured peak-to-peak voltage is more or less constant, GC measurements of $CO_{2,out}$ are taken. Hence, the CO_2 conversion is calculated as follows, based on the moles of CO_2 converted/moles of CO_2 introduced (first part of Eq. (1)):

$$X_{CO_2} = \frac{CO_{2,in} - CO_{2,out}}{CO_{2,in}} \times 100\% = \frac{CO_{out}}{CO_{out} + CO_{2,out}} \times 100\% \quad (1)$$

Table 1
Different parameters studied, as well as their variation.

VariationParameters studied				
Packing morphology	Glass wool	Quartz wool	Dielectric beads	
Gap size (mm)	2	2.5	3.5	4.5
Bead size for fixed bead/gap size ratio (±0.6) experiments (mm) (only $BaTiO_3$ spheres)	1.18–1.25	1.4–1.6	2.0–2.24	
Dielectric barrier material	Quartz	Alumina		
Dielectric bead material	SiO_2	ZrO_2	Al_2O_3	$BaTiO_3$
Bead size (mm) for the different materials, at fixed gap size of 4.5 mm	1.25–1.4	1.6–1.8	2.0–2.24	

We consider the dissociation of CO_2 in CO and ½O_2 as the only reaction taking place in our reactor. This can be explained as follows: the formation of O_3 cannot be detected with the GC, but for the four different bead materials, the formation of ozone was tested during 1 experiment with ozone detector tubes (Kitagawa tubes 182SA 50-1000 ppm and 182SB 2,5-100 ppm, UK). During these tests, no ozone was measured after 40 minutes of plasma stabilisation, when measuring at the vent. Thus, although there was no systematic evaluation of ozone formation for all experiments performed, we are quite confident that no ozone was formed in either of the other experiments.

Moreover, since there is no coking on the inner electrode, dielectric barrier or packing beads, the formation of solid C can be excluded. Furthermore, results obtained by calculating the conversion based on CO_2 content in feed and unconverted CO_2 in the exhaust gas (first part of Eq. (1)) and based on CO and unconverted CO_2 content in the exhaust gas (second part of Eq. (1)) are within experimental error. Thus, CO_2 is indeed selectively converted into CO and O_2.

This formula (Eq. (1)) takes the densities of the molecules into consideration, and not the differing velocities of the species at the inlet and the outlet of the reactor (see Eq. (17), Ref. [63]). Since CO_2 is split into CO and ½O_2 in this work, without the formation of a substantial amount of other molecules (such as O_3), every converted CO_2 molecule gives rise to an expansion of the volume by a factor 1.5. As we have a fixed volume sample loop and the GC depressurizes to 1 atm. for each measurement, the actual outlet flow measured is lower than the inlet flow. Hence, the conversion measured by the GC will not be the actual conversion. To correct for this, we adapted the equation of Ref. [63], based on the mass flow conservation and taking into account a constant reactor tube cross section, to the following formula:

$$X_{GC} = \frac{2X_{CO2}}{3 - X_{CO2}} \tag{2}$$

More details about the meaning and use of this correction factor and formula can be found in the work of Pinhão et al. [64].Based on this real conversion (corrected Xco_2, X_{GC}), the energy efficiency of the process can be calculated. The following formula is used for this purpose:

$$\eta(\%) = \frac{\Delta H_r(\frac{kJ}{mol}) * X_{CO_2}(\%)}{SEI(\frac{kJ}{L}) * 22.4(\frac{L}{mol})} \tag{3}$$

ΔH_R is the reaction enthalpy of CO_2 dissociation (i.e., 279.8 kJ/-mol), X_{CO2} is the amount of CO_2 converted, determined from Eqs. (1) and (2), and SEI is the specific energy input in the plasma, defined as:

$$SEI\left(\frac{kJ}{L}\right) = \frac{PlasmaPower(kW)}{FlowRate(\frac{L}{\min})} * 60\left(\frac{s}{\min}\right) \tag{4}$$

The gas flow rate is in all experiments either 50 ml/min or 192 ml/min. More specifically, for the experiments with packing, the flow rate is always kept fixed at 50 ml/min, but in the empty reactor, experiments are performed both at 50 ml/min (same flow rate) and at 192 ml/min (same residence time as in the packed bed reactor). The reasoning behind this is that inserting a packing in the reactor reduces the reactor volume and thus the residence time at constant flow rate. For different bead sizes, the reduction in reactor volume is constant [65]. When different gap sizes are investigated, the reactor volume is no longer constant and therefore, the residence time changes.

The power in the above formula is the power supplied to the plasma, i.e., the so-called plasma power, as is most common in literature [28,34,66–68]. The applied power is kept fixed at 100 W, as mentioned above, but the actual plasma power can be slightly different for each gas composition, and is obtained by means of the Lissajous figures (see Supporting information for more details).

Analysing the Lissajous figures is a common method for the investigation of the electrical characteristics in a DBD [40,69–71].

2.2. Packing materials

As mentioned before, the packing inserted in the plasma reactor is either glass wool (VWR, Belgium), quartz wool (Quantachrome, Germany) or spherical beads. The SiO_2 (soda lime glass) and ZrO_2 (Y stabilised) beads are purchased at SiLiBeads (Germany). The $BaTiO_3$ beads are supplied by Catal (UK), while the Al_2O_3 beads are made in-house at VITO.

Indeed, to warrant high sphericity of the Al_2O_3 beads in combination with a narrow and controlled size distribution in the ranges applied in this work, Al_2O_3 spheres were produced via a controlled shaping process. The shaping process was done via vibrational droplet coagulation with a Spheronisator M from Brace GmbH (Germany). The synthesis procedure is based on a recently developed method using alginate based droplet coagulation to shape ceramic Al_2O_3 particles [72].

The ceramic suspension is made of sodium alginate (0.53%), water (49.38%), Darvan C (a dispersant, 0.23%) and Al_2O_3 powder (49.86%, α-Al_2O_3 A16 SG purchased from Almatis with a d_{50} of 0.5 μm and specific surface area of 9 m^2/g.). The coagulation bath contains a 4 wt.% $CaCl_2$ and isopropanol is, if needed, added to lower the surface tension. After formation, thermal treatment is performed: drying at 100 °C for 4 h followed by calcination and sintering. All organic additives are thus removed. Sinter procedure: room temperature to 600 °C at a rate of 120 °C/h, hold 600 °C for 1 h, heat to 1490 °C at a rate of 180 °C/h, heat to 1540 °C at a rate of 60 °C/h, hold 1540 °C for 1 h, cool down at a rate of 120 °C/h).

The final characteristics of the α-Al_2O_3 spheres (9.2% $CaO.6Al_2O_3$) are a diameter of 1.4, 1.7 and 2.1 mm, obtained by using a nozzle of 0.9 mm, 0.7 mm and 1.2 mm.

The surface acidity of all spheres was determined by NH_3-TPD with a Quantachrome Autosorb-iQ-C equipped with a thermal conductivity detector (TCD). The procedure for NH_3-TPD is described elsewhere [73].

The open porosity of the spheres was measured by Mercury Intrusion Porosimetry (Pascal 140, Thermo Scientific, USA), which measures the pore size distribution and the pore volume [74]. The surface area was determined with N_2-sorption (Quantachrome QUADRASORB SI, USA), after degassing the samples at 150 °C for 16 h under high vacuum. The surface roughness was determined

with profilometry, for the 2.0–2.24 mm beads, and a Brücker Dektak XT stylus profiler was used for the 3D mappings. It was equipped with a 2 μm radius stylus and was controlled and analyzed with the Vision 64 software. The scans were performed on a 300 × 300 μm square with a stylus strength of 0.5 mg.

3. Results and discussion

3.1. Effect of bead material and bead size

3.1.1. General results

The influences of bead material (SiO_2, ZrO_2, Al_2O_3 and $BaTiO_3$) and bead size (ranges of 1.25–1.4, 1.6–1.8 and 2.0–2.24 mm diameter) are compared with the conversion and energy efficiency in the empty reactor (Fig. 2).

The first observation to be made is that $BaTiO_3$, for the three different bead sizes, yields a higher conversion than the empty reactor, for the same flow rate. Also the largest beads of Al_2O_3 yield a higher conversion than the empty reactor. Thus, in these cases, the positive contribution of the packing [43] compensates for the lower residence time. For SiO_2 and ZrO_2, as well as for the smaller beads of Al_2O_3, the CO_2 conversion is lower than in the empty reactor, illustrating that the packing effect does not compensate here for the lower residence time. When comparing at the same residence time (i.e., 5.52 s corresponding to 192 ml/min for the empty reactor), also Al_2O_3 systematically yields higher conversions, and in some cases, the conversion with ZrO_2 and SiO_2 beads is slightly higher as well. The highest values obtained are close to 20% conversion, for the Al_2O_3 and $BaTiO_3$ beads with the largest size.

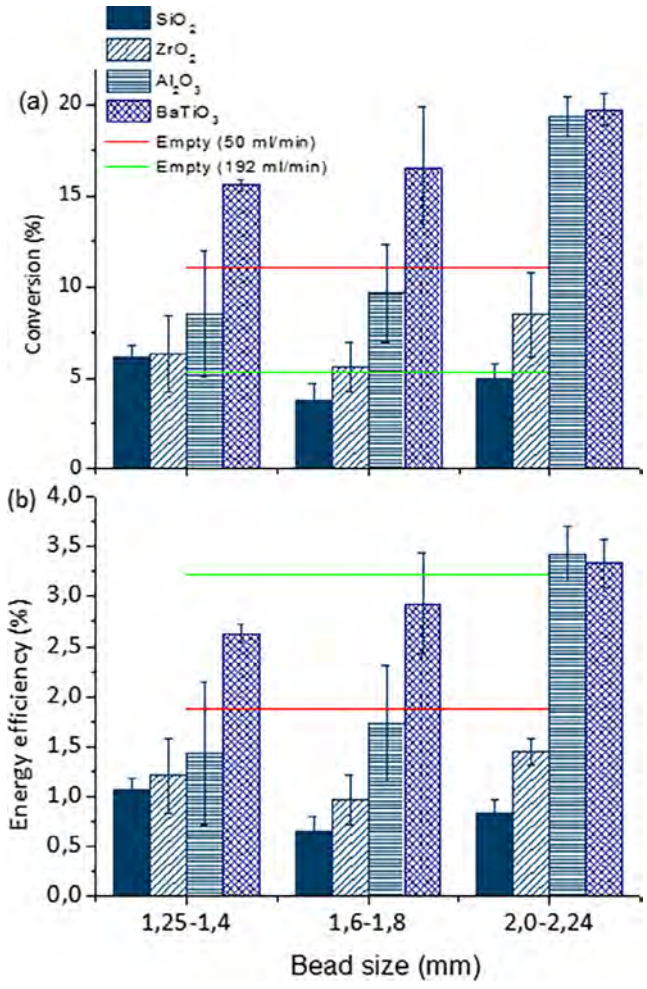

Fig. 2. Conversion (a) and energy efficiency (b) as a function of bead size (diameter) for different bead materials, for an alumina dielectric barrier, 4.5 mm gap, stainless steel outer electrode, 23.5 kHz, at 50 ml/min gas flow rate, and 100 Watt power. The error bars are calculated based on 12 GC measurements. Comparison is also made with the results for an empty reactor (i.e., without packing), both at the same flow rate (50 ml/min) and the same residence time as in the packed bed reactor (i.e., 5.52 s, corresponding to a flow rate of 192 ml/min).

For the energy efficiency (Fig. 2(b)), the same results are obtained as for the conversion when comparing at equal flow rate, i.e., only a higher energy efficiency is obtained for $BaTiO_3$, for the three different bead sizes, as well as for the largest beads of Al_2O_3. This is logical since the flow rate is part of the formula for calculating the energy efficiency out of the conversion (see Section 2.1). When comparing with the empty reactor at the higher flow rate of 192 ml/min (and thus the same residence time of 5.52 s), none of the packed bed results surmounts the energy efficiency of the empty reactor, as the higher flow rate yields a lower SEI, compensating for the lower conversion in the empty reactor, overall resulting in a higher energy efficiency. Nevertheless, for the largest bead sizes, both Al_2O_3 and $BaTiO_3$ have a similar and even slightly higher energy efficiency (3.5%) than the empty reactor at equal residence time (and thus higher flow rate), but, at the same time, they have a 4 times higher conversion, as is obvious from Fig. 2(a). This conversion and energy efficiency is roughly a factor 2 higher than in the empty reactor with the same flow rate. This coincides well with values reported in literature and is even slightly better. Indeed, in previous work from our group, the CO_2 conversion and energy efficiency were simultaneously enhanced by up to a factor 1.9 and 2.2, respectively, for ZrO_2 beads, compared to the values in an unpacked DBD reactor at the same flow rate [33,35]. Likewise, the conversion and energy efficiency for the dry reforming of methane were reported to double when adding a Ni/Al_2O_3 catalyst [75] (ratio gap/packing size is 10), while we observe that adding Al_2O_3 alone can already almost double the CO_2 conversion and energy efficiency. This means that the combination of plasma and these packing materials, with or without further catalytic activation, is very promising for improving the CO_2 conversion. Moreover, it emphasizes the importance of studying the properties-activity correlation of the packing materials itself (both chemical and structural properties), prior to further catalytic activation, in terms of improved conversion and energy efficiency, to identify the real impact of the catalytic element itself.

3.1.2. Effect of the material characteristics

To better understand the differences induced by the various materials, we looked at different material characteristics that might be correlated to their performance (Table 2). A first important observation is that none of the packing materials introduced in the reactor showed coking during the plasma experiments, which was confirmed with TGA measurements. The power introduced in the plasma reactor for the different packing materials, at a constant applied power of 100 W, is also mentioned in the table, as it is used to calculate the energy efficiency. If the plasma power for a certain packing material would be much higher for the same applied power, it could lead to a higher CO_2 conversion. However, as is clear from Table 2, the plasma power is very similar for the four different packing materials. The differences in plasma power with varying bead size are represented by the error bars.

Table 2 also shows the breakdown voltage as a function of the bead material. A higher dielectric constant should give rise to a higher electric field and thus a lower breakdown voltage. However, there is a plateau in increasing electric field with increasing dielectric constant [76], and therefore also in decreasing breakdown voltage. Since there is also an experimental error on the breakdown voltages measured, this can explain why e.g. the breakdown voltage of ZrO_2 is lower than the one of $BaTiO_3$.

Table 2
Material characteristics of the various beads used in this study.

	SiO_2	ZrO_2	Al_2O_3	$BaTiO_3$
Dielectric constant [77,78]	3.9	25	9.1	4000
Surface acidity (# sites/nm^2)[a]	0.27	≈0	≈0	≈0
Specific heat (J.g^{-1} K^{-1}) [79–82]	2.93	0.46	0.80	0.42
Molar heat (J.mol^{-1}.K^{-1})[b]	59.64	56.23	81.38	94.68
BET surface area (m^2/g)[c]	0.5	~ 0.0	0.1	0.8
Total open pore volume (mm^3/g)[d]	≈0	≈0	8.47	158.00
Pore size (μm) [d]	≈0	≈0	0.08	0.87
Plasma power (Watt)[e]	61 ± 1	57 ± 5	60 ± 4	61 ± 3
Breakdown voltage (kV)[e]	1.47	0.82	1.84	0.97
Surface roughness (nm)[f]	82 ± 3	84 ± 1	150 ± 4	590 ± 15

[a] Determined with NH_3-TPD, as explained in Section 2.2.
[b] Obtained from[80–83].
[c] Determined by N_2-sorption.
[d] Determined by Hg porosimetry, for 1.6–1.8 mm beads.
[e] Determined by analyzing the Lissajous figures.
[f] Determined by profilometry, for 2.0–2.24 mm beads. The profiles for the 4 different materials can be found in SI.

The results of Fig. 2 show a general trend (although some error bars overlap), with SiO_2 consistently yielding the lowest conversion and energy efficiency, followed by ZrO_2, Al_2O_3 and then $BaTiO_3$, inducing the highest conversion and energy efficiency. Therefore, the materials are listed in this order in the table. Important to note is that the relationship of size and its impact on conversion is not linear for any of the materials, nor is the correlation similar for the different materials, indicating that divergent and/or multiple interplaying mechanisms/properties are at the origin of these changes.

As mentioned in the introduction, the effect of the packing is usually correlated to the enhanced electric field at the contact points, due to polarization of the beads [33]. Hence, based on this, one would expect to see an increasing conversion and energy efficiency upon rising dielectric constant of the beads, as the latter typically gives rise to more pronounced electric field enhancements and higher electron temperatures [77]. As can be seen from Table 2, this correlation is only partially true for our results. Indeed, the conversion rises from SiO_2 (ε ~3.9) to $BaTiO_3$ (ε ~4000), but the results for ZrO_2 and Al_2O_3 do not follow this trend. Moreover, their size dependence is not the same. Even at the largest size, Al_2O_3 has the same conversion as $BaTiO_3$ even though the dielectric constant is much lower.

Van Laer et al. investigated both the influence of bead size and dielectric constant by modelling a helium discharge in a packed bed DBD reactor [76]. The modelling results illustrate that the dielectric constant of the beads influences the plasma density in the gap, the electric current profile, the electric field strength and the electron temperature, irrespective of the bead size.

Most importantly, upon increasing the dielectric constant, the time-averaged electric field strength is enhanced, which leads to a higher electron temperature, but a lower electron density, because the electrons get lost more easily at the walls. This will lead to a shift from full gap discharge to localized discharges upon rising dielectric constant of the beads. Moreover, at larger bead sizes, the shift from full gap discharge to localized discharges will occur at a higher dielectric constant, which can be explained through the larger voids in between the larger beads.

In this work, the highest conversion and energy efficiency were obtained with the largest $BaTiO_3$ beads. In accordance with the modelling results obtained by Van Laer et al., the electric field is enhanced upon increasing dielectric constant, but will not be enhanced further upon increasing bead size of $BaTiO_3$. On the other hand, larger beads will result in a higher electron density in the plasma. Therefore, the combination of a high dielectric constant and a large bead size will lead to a stronger electric field and the highest electron density, thus increasing the conversion and energy efficiency [76].

This electric field enhancement is also correlated to the surface roughness, also mentioned in Table 2. Although the increase in surface roughness appears in the same order as the increase in conversion and energy efficiency, there is no linear trend visible. Therefore, there must be other material characteristics that can influence the conversion and energy efficiency, like surface acidity, surface area, specific and molar heat capacity, total open pore volume and pore size, or others (Table 2) [84].

The number of acid sites was only measurable for SiO_2 and even here the value is quite low, making it not possible to correlate the results obtained with the surface acidity. Similarly, there is no correlation between the increase in conversion and energy efficiency with the molar or specific heat capacity. Since we add the same volume of spheres to each experiment, and thus the weight and number of moles differ, this explains the fact that there is no correlation.

Another characteristic that might play a role are the structural properties of the beads. There are 3 different characteristics that define the spheres: pores, edges through porosity and surface roughness. In general, the electric field may be enhanced by some form of roughness or geometric distortion in the reactor, and this enhancement of the electric field strength can cause a higher conversion and energy efficiency [36].

The first two characteristics both correlate to the porosity of the beads. The porosity of Al_2O_3 is created in the manufacturing process, since all beads here are sintered at 1540 °C, creating minor porosities in the Al_2O_3 spheres. As the other beads are purchased, we cannot conclude on the manufacturing of the spheres and thus Hg porosimetry was conducted. SiO_2 and ZrO_2 have a very low porosity, whereas Al_2O_3 and $BaTiO_3$ have a higher porosity (Table 2). The pore size distributions for Al_2O_3 and $BaTiO_3$ are illustrated in Fig. 3. The results indicate that the Al_2O_3 spheres have a pore size distribution with an average pore diameter of 0.08 μm, whereas the $BaTiO_3$ spheres mainly have pores with a diameter of 0.87 μm, which is more than tenfold the value of the Al_2O_3 beads. According to model calculations (for a helium plasma) carried out in our group, a pore diameter of 0.87 μm is too small for plasma generation inside the pores [85], although streamers might still be able to penetrate [86], and especially the edges induced by the porosity can still enhance the electric field and thus influence the results for conversion and energy efficiency. Although multiple parameters will be different and could be the underlying reason, these differences might contribute to the rise in CO_2 conversion and energy efficiency for both Al_2O_3 as well as $BaTO_3$.

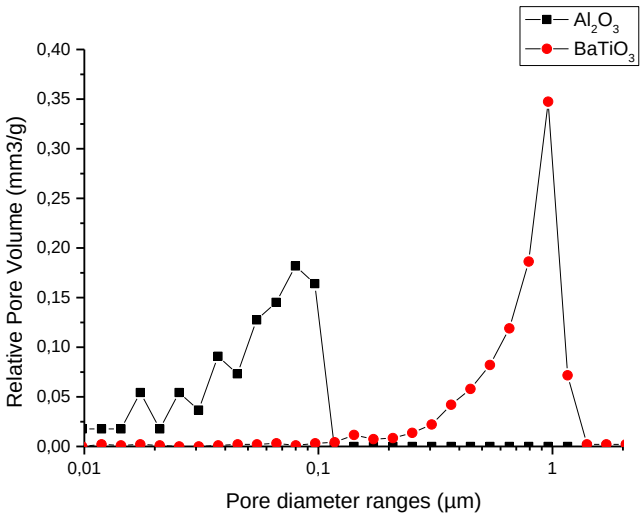

Fig. 3. Relative pore volume for Al_2O_3 and $BaTiO_3$ beads.

It is clear from the above results that the conversion and energy efficiency are not only correlated to the dielectric constant of the packing beads, but also to other material properties. However, in order to draw final conclusions on the exact influence of the material properties, further thorough research needs to be conducted in a systematic way, based on materials with very controlled material properties, which can only be obtained by careful manufacturing of the beads instead of using commercial beads. This controlled manufacturing process is also not straightforward [72], and requires more investigation, so this will be the subject of our future work.

3.1.3. Effect of the bead size

Fig. 2 shows a clear influence of the bead size affecting the conversion and energy efficiency. Moreover, the results differ depending on the packing material inserted in the DBD. SiO_2 and ZrO_2, show no clear (linear) trend of bead size. For SiO_2, the conversion and energy efficiency increase in the following order: 1.6–1.8 mm < 2.0–2.24 mm < 1.25–1.4 mm, while for ZrO_2, the results rise in the following order: 1.6–1.8 mm < 1.25–1.4 mm < 2.0–2.24 mm. On the other hand, for Al_2O_3 and $BaTiO_3$, the results increase upon increasing bead size (1.25–1.4 mm < 1.6–1.8 mm < 2.0–2.24 mm). Note, however, that the exact trends have to be considered with caution, as some of the error bars overlap.

There are multiple possible explanations as to why the effect of bead size is different for the different bead materials.

Firstly, the electric field enhancement in the reactor due to the packing is expected to give rise to a higher conversion and energy efficiency. This electric field enhancement is attributed to polarization effects and the accumulation of charges on the surface of the (dielectric) beads. It is governed by the contact angle, the curvature and the dielectric constant of the beads. Moreover, there are more contact points between the smaller beads (and also between the beads and the dielectric barrier), and the electric field enhancement takes place at these contact points [33,43]. Hence, one could expect that smaller beads would give rise to a higher conversion and energy efficiency but due to its dependence on dielectric constant, differences might be present. Modelling results show a higher electric field for smaller beads, and a higher overall enhancement for packing beads with a higher dielectric constant, indicating that trends can indeed be different, based on both the size and dielectric constant of the beads [76].

Secondly, since the discharges take place in the voids between the beads and larger bead sizes have larger void spaces, the electrons are not so easily adsorbed at the surfaces of the beads, so there are more electrons available for electron impact dissociation of CO_2, which can lead to a higher conversion and energy efficiency. This would mean that larger beads can give rise to a higher conversion and energy efficiency. Depending on which effect is dominant, the final result in conversion or energy efficiency will be higher for either the smaller or the larger beads. The latter appears to be material-dependent, which is not unexpected, because the electric field enhancement is determined by the dielectric constant of the materials. Nevertheless, to be able to exclude other effects, further research through modelling and studies with more controlled material properties are required to confirm the extent of these effects.

3.2. Combined effect of bead size and gap size

The experiments for the combined influence of gap size and bead size are conducted with the $BaTiO_3$ beads, for which the best results are obtained, at 50 ml/min. Results are shown for (1) a constant ratio between average bead size and gap size but with varying dimensions; (2) a constant bead size but a varying gap, and (3) vice versa (already shown in Fig. 2). Table 3 summarizes the combinations of gap size and bead size investigated.

As is clear from Fig. 4, the conversion and energy efficiency rise upon increasing gap size and bead size, as long as the ratio between both is constant (cf. the first 3 data points). The values increase from 18% to 26% conversion, and from 3% to 4% energy efficiency. When comparing column 3 and 4 in Fig. 4, using the same bead size but a larger gap size and thus a lower ratio bead/-gap size (hence allowing slightly more beads in the same gap), we can observe that the conversion and energy efficiency decrease again. In addition, at a fixed gap (4.5 mm), increasing the bead size from 1.25–1.4 to 2.0–2.24 mm resulted in an increase of conversion and energy efficiency, as observed in Fig. 2. The maximum conversion (20%) and energy efficiency (~3.7%) obtained in this case, however, are lower than the conversion and energy efficiency in the smaller gap size of 3.5 mm. Hence, it is clear that in order to optimize the conversion and energy efficiency, the bead size and gap size have to be adjusted to each other. The same is seen in a paper by Van Laer and Bogaerts [33], who found that the ideal ratio between ZrO_2 spheres and the gap size is higher than 1/3rd. Since our results are only obtained for $BaTiO_3$ and for few data points, no general conclusions can be drawn.

Nevertheless, it is important to state that all the above aspects are important to take into account: the gap size, the void spaces in between the beads, the surface to volume ratio, the number of contact points between the beads, and between the beads and the dielectric barrier, as they are all influencing the conversion and energy efficiency. For instance, the relative rise in conversion and energy efficiency upon increasing bead size (from 1.18–1.25 mm to 2–2.24 mm) is 40% and 33% (i.e., from 18 to 26% conversion and from 3 to 4% energy efficiency) in the case of constant bead size/gap size ratio, while it is 27% (i.e., from 16 to 20% conversion and from 2.6 to 3.3% energy efficiency) in case of constant gap size,

Table 3
Parameters used for investigating the influence of the gap size and bead size, at equal ratio, bead size or gap size.

Bead size range	Gap size	Ratio
1.18–1.25	2	0.6075
1.4–1.6	2.5	0.6000
2.0–2.24	3.5	0.6057
2.0–2.24	4.5	0.4711
1.6–1.8	4.5	0.3777
1.25–1.4	4.5	0.2944

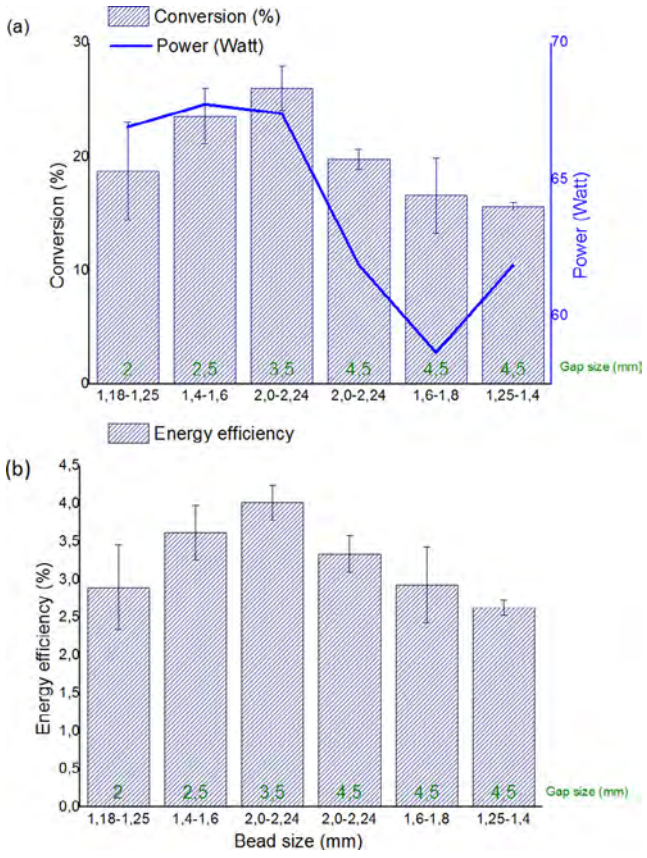

Fig. 4. Conversion (a) and energy efficiency (b) as a function of bead size and gap size (indicated at the bottom of the columns, in mm), for $BaTiO_3$ beads, an alumina dielectric barrier, stainless steel outer electrode, 23.5 kHz, at 50 ml/min, for 100 Watt input power. The plasma power (Watt) is indicated by a blue line.

for the same rise in bead size. The stronger rise upon increasing bead size at constant bead/gap size ratio might be caused by the constant number of beads and thus contact points, while in the case of constant gap size, the number of contact points will drop upon increasing bead size.

Ideally, a packing material should thus have large voids present between the particles, allowing less electron losses, in balance with a large number of contact points and an adjusted gap size to have a maximum enhancement of the electric field. Following this conclusion, it could be interesting to investigate even larger bead sizes, along with larger gap sizes, although this might not be beneficial in terms of plasma catalysis, as it will yield a lower catalyst surface area. Hence, there will be an optimum combination, keeping in mind both physical and chemical (surface) effects.

The power indicated on Fig. 4 only varies between 58.6 and 67.7 Watt, and does not follow the same trend as the conversion or energy efficiency. Therefore, the results obtained here cannot be explained through a variation of the actual plasma power.

The change in the power itself can be explained through the losses caused by transferring the power from the power supply to the reactor. Since this is a very unstable process, the power changes a little over the different conditions.

3.3. Effect of glass wool or quartz wool packing

Duan et al. performed experiments with a quartz wool packed DBD reactor [49] and reported that the insertion of quartz wool yields better results, in terms of conversion, than inserting beads of different materials and sizes. As we always use glass wool to fix the packing material in our reactor, we measured the influence of both glass and quartz wool packing in the reactor.

A first set of experiments compares a completely empty reactor, a reactor with glass wool, but only outside of the discharge zone, and a reactor completely filled with glass wool. The experiments are carried out at two different flow rates, i.e. 50 and 192 ml/min. The results for conversion and energy efficiency are plotted in Fig. 5 The plasma power for these experiments is (67 ± 2) Watt.

We can see that, when taking the error bars into account, there is no significant effect of inserting glass wool in the reactor. The effect is negligible for both energy efficiency and conversion. The conversion is around 10–11% at a flow rate of 50 ml/min, and around 5–6% at a flow rate of 192 ml/min, while the energy efficiency is about 1.7–1.9% and 3–4% for the gas flow rates of 50 and 192 ml/min, respectively. In Section 3.1 above, we already observed that SiO_2 beads have a negative effect on the conversion and energy efficiency, compared to an empty reactor, since the enhancement of the electric field is too limited, probably due to the low dielectric constant. Hence, it seems that the improvement, which might be expected from the enhanced electric field at the contact points and edges of the glass wool packing, is entirely compensated by the reduction in residence time of the packed reactor, which of course limits the conversion and thus the energy efficiency.

Our results are thus different from the ones obtained by Duan et al., where an improved conversion was reported in case of a quartz wool packing [49]. Note, however, that our setup differs from the one of Duan et al. in several aspects. Indeed, they used an aluminium foil as outer electrode, a much smaller gap size of 0.6 mm, a different frequency (18 kHz) and flow rate (19.8 ml/min).

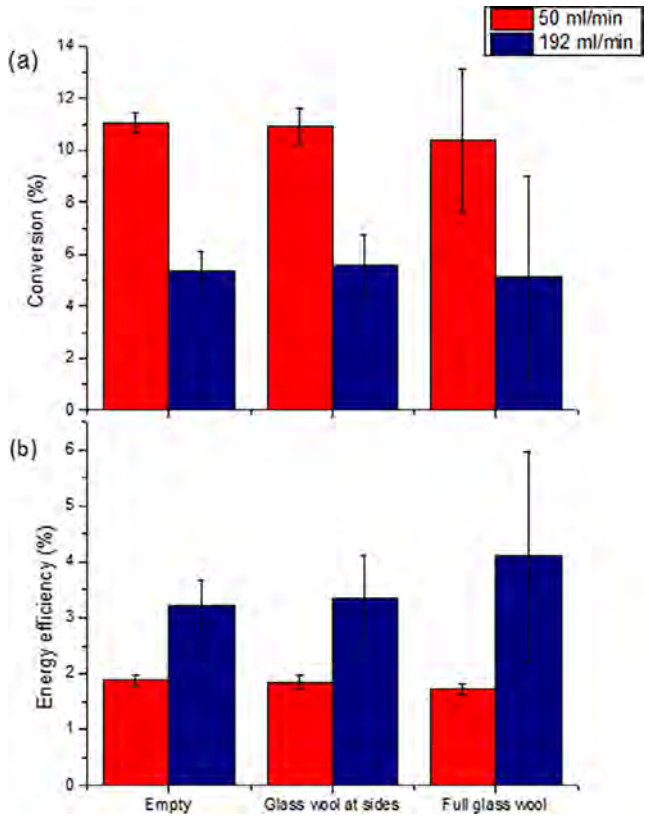

Fig. 5. Conversion (a) and energy efficiency (b) in an empty reactor (left), an empty reactor with glass wool at the sides (middle) and a reactor completely filled with glass wool (right) at two different flow rates, for 100 Watt power, alumina dielectric barrier, stainless steel electrode, at 23.5 kHz and 4.5 mm gap.

The major difference between our reactor setup and their reactor setup is the different gap size (i.e., 4.5 mm vs 0.6 mm), so it might be possible that the effects reported by Duan et al. only occur in a microgap. Therefore, we also performed additional experiments in a microgap reactor. The reactor setup is the same as used before, but different inner electrodes are used, with varying outer diameter and thus influencing the gap. The gap sizes obtained are 268 μm, 455 μm, 705 μm and 1230 μm. The results are summarised in Fig. 6. Note that the results in the 268–1230 μm gaps were obtained with different flow rates to yield the same residence time of about 7.5 s (in case of the packing), whereas the residence time in the 4.5 mm gap reactor was 5.5 s and it was 1 second in the experiments of Duan et al.

It can be clearly seen from Fig. 6 that the conversion for an empty reactor is higher than for a reactor filled with glass wool, in the case of a 268 μm gap and a 455 μm gap. However, for the 705 and 1230 μm gaps, the reactor filled with glass wool yields a significantly higher conversion than the empty reactor, in agreement with the results of Duan et al. for the quartz wool packing. This means that the influence of glass wool (or quartz wool) on the conversion is indeed gap size dependent, and this can explain the difference in results compared to Duan et al. Furthermore, it is obvious from Fig. 6 that the CO_2 conversion in the smaller gaps is larger. This can partially be explained by the enhanced electric field and electron temperature in the smaller gaps, as predicted by model calculations [77]. The effect of micrometer gap sizes in correlation to packing properties will be further investigated in our future work.

To exclude that the difference with the results of Duan et al. is attributed to the different packing material (i.e., glass wool vs quartz wool, as used by Duan et al.) or reactor material, we also performed a second set of experiments, comparing glass wool and quartz wool packing, as well as an alumina and quartz dielectric tube, to investigate the impact of the chemical nature of the dielectric tube as well, as in the experiments of Duan et al., quartz wool was applied in combination with a quartz dielectric barrier. The results for the conversion and energy efficiency are shown in Fig. 7.

Again, no significant difference in conversion or energy efficiency compared to the empty reactor, or among each other is observed, keeping in mind the error bars in the results. Therefore, these experiments show us that there is no influence of using quartz wool or glass wool as a packing material in the 4.5 mm gap reactor. Furthermore, it also indicates that, at least in our 4,5 mm gap reactor, we can use glass wool (or quartz wool) to fixate the spherical beads (as done in the other parts of this manuscript), without affecting the conversion or energy efficiency.

Our results are in correlation with literature results for dry reforming, where it was reported that the conversion of CH_4 was slightly improved by the addition of quartz wool to the discharge gap, from 23 to 27% at a discharge power of 30 W in comparison to an empty reactor, while the CO_2 conversion did not increase [40].

3.4. Interaction between dielectric barrier and bead material

Finally, the influence of the interaction between dielectric barrier material and bead material is studied by comparing the results for SiO_2 beads and Al_2O_3 beads of 1.6–1.8 mm diameter, both with a quartz and an alumina dielectric barrier. In this way we can compare all possible interactions between silica and alumina packing versus dielectric reactor tube. Fig. 8 illustrates that for both conversion and energy efficiency, there is no significant effect of altering the dielectric barrier material, while there is a significant effect when using SiO_2 or Al_2O_3 beads, as elaborated in Section 3.1 above. Thus, like for the glass wool and quartz wool packing (see previous section), the dielectric barrier seems to play only a minor role in the conversion and energy efficiency.

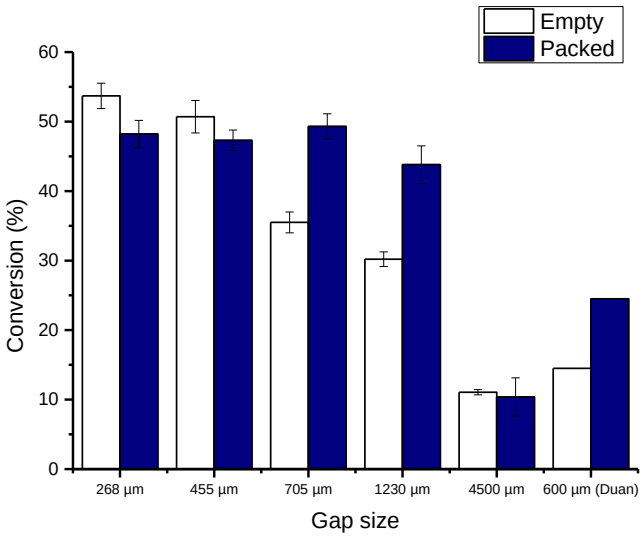

Fig. 6. Effect of a glass wool packing on the CO_2 conversion, for different gap sizes, in comparison with the results by Duan et al. for a quartz wool packing.

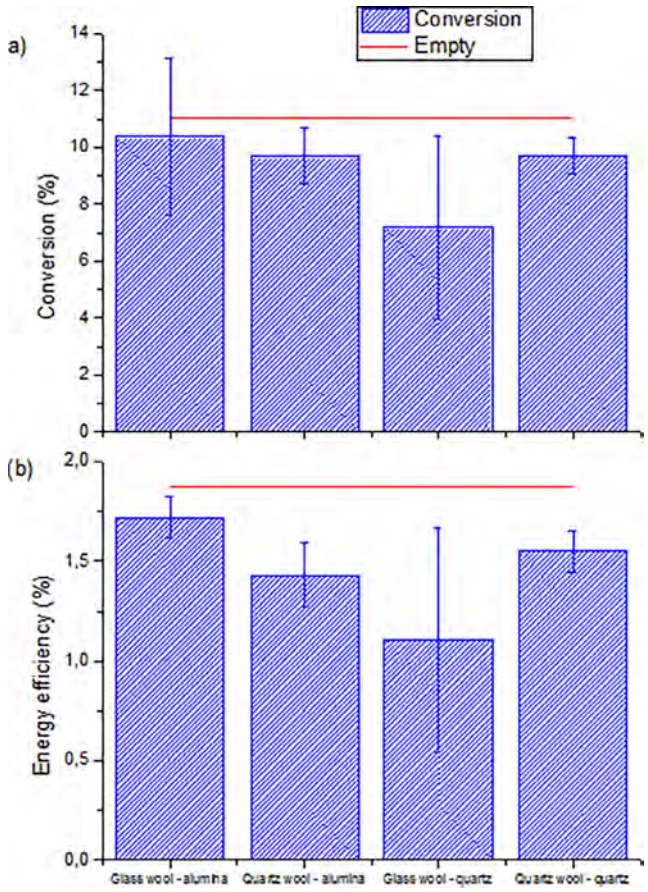

Fig. 7. Conversion (a) and energy efficiency (b) for two different dielectric barriers and packing materials, as indicated in the x-axis, at 50 ml/min, for 100 Watt power, 4.5 mm gap, 23.5 kHz and a stainless steel electrode.

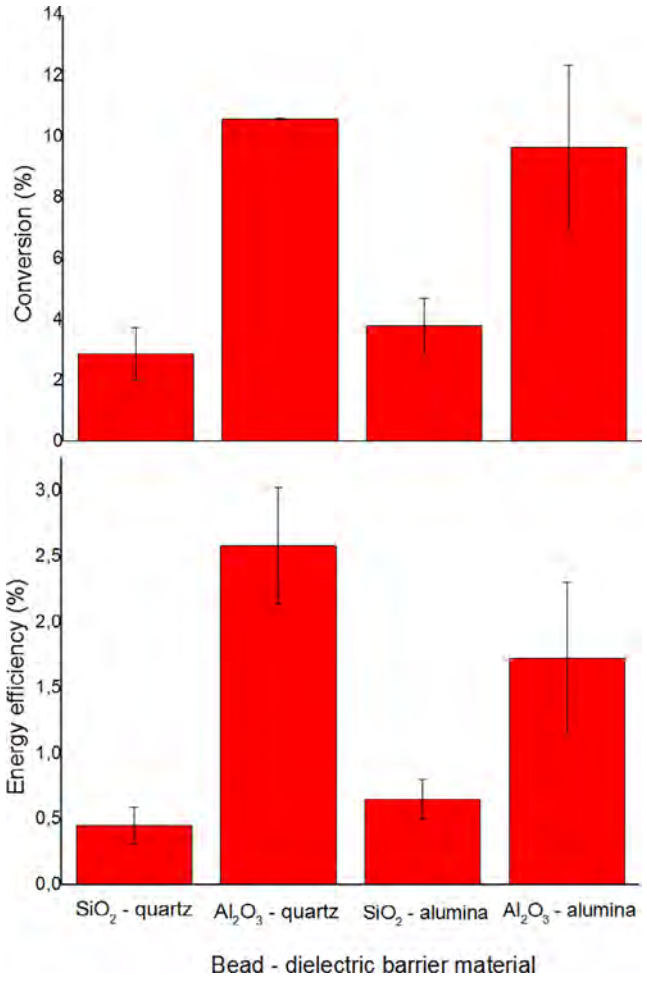

Fig. 8. Conversion (a) and energy efficiency (b) for silica and alumina spheres, with quartz and alumina dielectric barriers, at 50 ml/min, for 100 Watt power, 4.5 mm gap, 23.5 kHz and a stainless steel electrode.

4. Conclusion

We showed a clear influence of specific material and reactor properties on the conversion and energy efficiency of CO_2 dissociation in a packed bed DBD reactor. This indicates that correlating results from literature obtained in different setups is not straightforward and should be considered with care.

The highest obtained conversion in this work was 25%, with a corresponding energy efficiency of 4.5%. When comparing the results for different materials and bead sizes in the reactor gap of 4.5 mm, the highest conversion was roughly a factor 2 higher than in the empty reactor with the same flow rate, and a factor 4 higher than in the empty reactor with the same residence time. The energy efficiency was the same when compared at the higher flow rate, but again almost twice as high when compared at the same flow rate.

It is clear that three effects play a role: (1) the positive contribution of the packing, due to electric field enhancement at the contact points, (2) a negative contribution due to the lower residence time in the presence of a packing, and (3) the influence of the voids between particles, with a positive or negative effect depending on the material inserted. Depending on the bead size and material, one or the other effect will dominate, explaining their different behaviour in conversion and energy efficiency. The changes in conversion can only partially be related to the dielectric constant of the beads, indicating that also other material parameters must play a role. In general, our results indicate that material performances should be compared with similar reactor setups as the latter have a vast impact on the materials influence. Further improvement in conversion and energy efficiency can be expected when a large number of contact points can be generated, while maintaining large void space volumes and a large ratio of bead size/gap size.

Finally, when searching for the most optimal catalyst, the impact of the packing material (chemistry and physical properties) itself, apart from the catalytic activation, cannot be neglected, since it can on itself already significantly improve the conversion and energy efficiency. This shows the large area of further improvement that relies in packed bed plasma reactors for CO_2 conversion and for other chemical conversion reactions.

Author contributions

Inne Michielsen conceived, designed and performed the experiments, with practical help from Yannick Uytdenhouwen. He also performed the microgap experiments. Judith Pype and Bart Michielsen assisted with the shaping of the alumina beads, the characterisation thereof and the Hg porosimetry and XRD measurements. François Reniers and Jeremy Mertens performed the profilometry measurements. Inne Michielsen wrote the paper; Vera Meynen and Annemie Bogaerts guided the work, modified the paper and discussed the results and explanations.

Acknowledgments

This research was carried out with financial support of the Institute for the Promotion of Innovation by Science and Technology in Flanders (IWT Flanders) for both I. Michielsen (IWT-141093) and J. Pype (IWT-131229) and of the Walloon region through the excellence programme FLYCOAT (nr. 1318147) for the profilometry measurements. The authors also acknowledge financial support from an IOF-SBO project from the University of Antwerp and from the Fund for Scientific Research (FWO; grant number: G.0254.14 N). This research was carried out in the framework of the network on Physical Chemistry of Plasma-Surface Interactions - Interuniversity Attraction Poles, phase VII (http://psi-iap7.ulb.ac.be/), and supported by the Belgian Science Policy Office (BELSPO).

The authors would also like to thank Koen Van Laer for the discussions on this manuscript.

Appendix A. Supplementary data

Supplementary data associated with this article can be found, in the online version, at http://dx.doi.org/10.1016/j.cej.2017.05.177.

References

[1] S. Perathoner, G. Centi, CO_2 recycling: a key strategy to introduce green energy in the chemical production chain, ChemSusChem 7 (2014) 1274–1282, http://dx.doi.org/10.1002/cssc.201300926.

[2] G. Centi, E.A. Quadrelli, S. Perathoner, Catalysis for CO_2 conversion: a key technology for rapid introduction of renewable energy in the value chain of chemical industries, Energy Environ. Sci. 6 (2013) 1711–1731, http://dx.doi.org/10.1039/c3ee00056g.

[3] M. Aresta, in: Carbon Dioxide as Chemical Feedstock, Wiley-VCH Verlag GmbH & Co. KGaA, Weinheim, Germany, 2010, http://dx.doi.org/10.1002/9783527629916.

[4] A. Lebouvier, S.A. Iwarere, P. D'Argenlieu, D. Ramjugernath, L. Fulcheri, Assessment of carbon dioxide dissociation as a new route for syngas production: a comparative review and potential of plasma-based technologies, Energy Fuels 27 (2013) 2712–2722, http://dx.doi.org/10.1021/ef301991d.

[5] J. Van Durme, J. Dewulf, C. Leys, H. Van Langenhove, Combining non-thermal plasma with heterogeneous catalysis in waste gas treatment: a review, Appl. Catal. B Environ. 78 (2008) 324–333, http://dx.doi.org/10.1016/j.apcatb.2007.09.035.

[6] H.H. Kim, A. Ogata, in: Interaction of Nonthermal Plasma with Catalyst for the Air Pollution Control, 2011, pp. 43–48.
[7] S.S. Kim, S.M. Lee, S.C. Hong, A study on the reaction characteristics of CO_2 decomposition using iron oxides, J. Ind. Eng. Chem. 18 (2012) 860–864, http://dx.doi.org/10.1016/j.jiec.2011.11.141.
[8] D. Dardor, R. Bhosale, S. Gharbia, A. Kumar, F. AlMomani, Solar carbon production via thermochemical ZnO/Zn carbon dioxide dissociation cycle, J. Emerg. Trends Eng. Appl. Sci. 6 (2015) 129–135.
[9] R. Snoeckx, R. Aerts, X. Tu, A. Bogaerts, Plasma-based dry reforming: a computational study ranging from nanoseconds to seconds timescale, J. Phys. Chem. 117 (2013) 4957–4970, http://dx.doi.org/10.1021/jp311912b.
[10] L. Yu, X. Tu, X. Li, Y. Wang, Y. Chi, J. Yan, Destruction of acenaphthene, fluorene, anthracene and pyrene by a dc gliding arc plasma reactor, J. Hazard. Mater. 180 (2010) 449–455, http://dx.doi.org/10.1016/j.jhazmat.2010.04.051.
[11] R. Aerts, X. Tu, C. De Bie, J.C. Whitehead, A. Bogaerts, An investigation into the dominant reactions for ethylene destruction in non-thermal atmospheric plasmas, Plasma Process. Polym. 9 (2012) 994–1000, http://dx.doi.org/10.1002/ppap.201100168.
[12] A.M. Harling, D.J. Glover, J.C. Whitehead, K. Zhang, Novel method for enhancing the destruction of environmental pollutants by the combination of multiple plasma discharges, Environ. Sci. Technol. 42 (2008) 4546–4550, http://dx.doi.org/10.1021/es703213p.
[13] X. Tu, J.C. Whitehead, Plasma dry reforming of methane in an atmospheric pressure AC gliding arc discharge: co-generation of syngas and carbon nanomaterials, Int. J. Hydrogen Energy 39 (2014) 9658–9669, http://dx.doi.org/10.1016/j.ijhydene.2014.04.073.
[14] X. Tu, J.C. Whitehead, Plasma-catalytic dry reforming of methane in an atmospheric dielectric barrier discharge: understanding the synergistic effect at low temperature, Appl. Catal. B Environ. 125 (2012) 439–448, http://dx.doi.org/10.1016/j.apcatb.2012.06.006.
[15] X. Tu, H.J. Gallon, M.V. Twigg, P.A. Gorry, J.C. Whitehead, Dry reforming of methane over a Ni/Al2O3 catalyst in a coaxial dielectric barrier discharge reactor,, J. Phys. D Appl. Phys. 44 (2011) 274007, http://dx.doi.org/10.1088/0022-3727/44/27/274007.
[16] S. Paulussen, B. Verheyde, X. Tu, C. De Bie, T. Martens, D. Petrovic, A. Bogaerts, B. Sels, Conversion of carbon dioxide to value-added chemicals in atmospheric pressure dielectric barrier discharges, Plasma Sources Sci. Technol. 19 (2010) 34015, http://dx.doi.org/10.1088/0963-0252/19/3/034015.
[17] R. Aerts, T. Martens, A. Bogaerts, Influence of vibrational states on CO_2 dissociation by dielectric barrier discharges, J. Phys. Chem. C 116 (2012) 23257–23273, http://dx.doi.org/10.1021/jp307525t.
[18] G. Horváth, J.D. Skalný, N.J. Mason, FTIR study of decomposition of carbon dioxide in dc corona discharges, J. Phys. D. Appl. Phys. 41 (2008) 225207, http://dx.doi.org/10.1088/0022-3727/41/22/225207.
[19] S.L. Brock, M. Marquez, S.L. Suib, Y. Hayashi, H. Matsumoto, Plasma decomposition of CO_2in the presence of metal catalysts, J. Catal. 180 (1998) 225–233, http://dx.doi.org/10.1006/jcat.1998.2258.
[20] J. Wang, G. Xia, A. Huang, S. Suib, CO_2 decomposition using glow discharge plasmas, J. Catal. 159 (1999) 152–159, http://dx.doi.org/10.1006/jcat.1999.2499.
[21] M. Tsuji, T. Tanoue, K. Nakano, Y. Nishimura, Decomposition of CO_2 into CO and O in a microwave-excited discharge flow of CO_2/He or CO_2/Ar mixtures, Chem. Lett. 1 (2001) 22–23, http://dx.doi.org/10.1246/cl.2001.22.
[22] T. Mikoviny, M. Kocan, S. Matejcik, N.J. Mason, J.D. Skalny, Experimental study of negative corona discharge in pure carbon dioxide and its mixtures with oxygen, J. Phys. D. Appl. Phys. 37 (2004) 64–73, http://dx.doi.org/10.1088/0022-3727/37/1/011.
[23] A. Indarto, D.R. Yang, J.-W. Choi, H. Lee, H.K. Song, Gliding arc plasma processing of CO_2 conversion, J. Hazard. Mater. 146 (2007) 309–315, http://dx.doi.org/10.1016/j.jhazmat.2006.12.023.
[24] L.F. Spencer, A.D. Gallimore, Efficiency of CO_2 dissociation in a radio-frequency discharge, Plasma Chem. Plasma Process. 31 (2011) 79–89, http://dx.doi.org/10.1007/s11090-010-9273-0.
[25] L.-T. Hsieh, W.-J. Lee, C.-T. Li, C.-Y. Chen, Y.-F. Wang, M.-B. Chang, Decomposition of carbon dioxide in the RF plasma environment, J. Chem. Technol. Biotechnol. 73 (1998) 432–442, http://dx.doi.org/10.1002/(SICI)1097-4660(199812)73:4<432::AID-JCTB972>3.0.CO;2-0.
[26] T. Nunnally, K. Gutsol, A. Rabinovich, A. Fridman, A. Gutsol, A. Kemoun, Dissociation of CO_2 in a low current gliding arc plasmatron, J. Phys. D. Appl. Phys. 44 (2011) 274009, http://dx.doi.org/10.1088/0022-3727/44/27/274009.
[27] H.J. Gallon, Dry Reforming of Methane Using Non-thermal Plasma-Catalysis, 2010.
[28] R. Aerts, W. Somers, A. Bogaerts, Carbon dioxide dissociation in a dielectric barrier discharge plasma: a combined experimental and computational study, ChemSusChem 8 (2015) 702–716, http://dx.doi.org/10.1002/cssc.201402818.
[29] H.L. Chen, H.M. Lee, S.H. Chen, M.B. Chang, S.J. Yu, S.N. Li, Removal of volatile organic compounds by single-stage and two-stage plasma catalysis systems: a review of the performance enhancement mechanisms, current status, and suitable applications, Environ. Sci. Technol. 43 (2009) 2216–2227, http://dx.doi.org/10.1021/es802679b.
[30] H.L. Chen, H.M. Lee, S.H. Chen, Y. Chao, M.B. Chang, Review of plasma catalysis on hydrocarbon reforming for hydrogen production—Interaction, integration, and prospects, Appl. Catal. B Environ. 85 (2008) 1–9, http://dx.doi.org/10.1016/j.apcatb.2008.06.021.
[31] J.C. Whitehead, Plasma catalysis: a solution for environmental problems, Pure Appl. Chem. 82 (2010) 1329–1336, http://dx.doi.org/10.1351/PAC-CON-10-02-39.
[32] E.C. Neyts, K. Ostrikov, M.K. Sunkara, A. Bogaerts, Plasma catalysis: synergistic effects at the nanoscale, Chem. Rev. 115 (2015) 13408–13446, http://dx.doi.org/10.1021/acs.chemrev.5b00362.
[33] K. Van Laer, A. Bogaerts, Improving the conversion and energy efficiency of carbon dioxide dissociation in a zirconia-packed dielectric barrier discharge reactor, Energy Technol. 3 (2015) 1038–1044, http://dx.doi.org/10.1002/ente.201500127.
[34] Y. Zeng, X. Zhu, D. Mei, B. Ashford, X. Tu, Plasma-catalytic dry reforming of methane over γ-Al_2O_3 supported metal catalysts, Catal. Today 256 (2015) 80–87, http://dx.doi.org/10.1016/j.cattod.2015.02.007.
[35] A. Bogaerts, T. Kozák, K. van Laer, R. Snoeckx, Plasma-based conversion of CO_2: current status and future challenges, Faraday Discuss. (2015) 217–232, http://dx.doi.org/10.1039/C5FD00053J.
[36] E.C. Neyts, A. Bogaerts, Understanding plasma catalysis through modelling and simulation—a review, J. Phys. D. Appl. Phys. 47 (2014) 224010, http://dx.doi.org/10.1088/0022-3727/47/22/224010.
[37] J. Sentek, K. Krawczyk, M. Młotek, M. Kalczewska, T. Kroker, T. Kolb, A. Schenk, K.-H. Gericke, K. Schmidt-Szałowski, Plasma-catalytic methane conversion with carbon dioxide in dielectric barrier discharges, Appl. Catal. B Environ. 94 (2010) 19–26, http://dx.doi.org/10.1016/j.apcatb.2009.10.016.
[38] H.K. Song, J.-W. Choi, S.H. Yue, H. Lee, B.-K. Na, H.K. Songu, Synthesis gas production via dielectric barrier discharge over Ni/γ-Al_2O_3 catalyst, Catal. Today 89 (2004) 27–33, http://dx.doi.org/10.1016/j.cattod.2003.11.009.
[39] M. Kraus, W. Egli, K. Haffner, B. Eliasson, U. Kogelschatz, A. Wokaun, Investigation of mechanistic aspects of the catalytic CO_2 reforming of methane in a dielectric-barrier discharge using optical emission spectroscopy and kinetic modeling, Phys. Chem. Chem. Phys. 4 (2002) 668–675, http://dx.doi.org/10.1039/b108040g.
[40] H.J. Gallon, X. Tu, J.C. Whitehead, Effects of reactor packing materials on H_2 production by CO_2 reforming of CH4 in a dielectric barrier discharge, Plasma Process. Polym. 9 (2012) 90–97, http://dx.doi.org/10.1002/ppap.201100130.
[41] L.F. Spencer A.D. Gallimore CO2 dissociation in an atmospheric pressure plasma/catalyst system: a study of efficiency Plasma Sources Sci. Technol. 22 2013 15019 10.1088/0963-0252/22/1/015019
[42] H. Lee, H. Sekiguchi, Plasma–catalytic hybrid system using spouted bed with a gliding arc discharge: CH_4 reforming as a model reaction, J. Phys. D. Appl. Phys. 44 (2011) 274008, http://dx.doi.org/10.1088/0022-3727/44/27/274008.
[43] K. Van Laer, A. Bogaerts, Fluid modelling of a packed bed dielectric barrier discharge plasma reactor, Plasma Sources Sci. Technol. 25 (2016) 15002, http://dx.doi.org/10.1088/0963-0252/25/1/015002.
[44] H.L. Chen, H.M. Lee, S.H. Chen, Review of packed-bed plasma reactor for ozone generation and air pollution control, Ind. Eng. Chem. Res. 47 (2008) 2122–2130, http://dx.doi.org/10.1021/ie071411s.
[45] A. Ozkan, T. Dufour, A. Bogaerts, F. Reniers, How do the barrier thickness and dielectric material influence the filamentary mode and CO_2 conversion in a flowing DBD?, Plasma Sources Sci Technol. 25 (2016) 18, http://dx.doi.org/10.1088/0963-0252/25/4/045016.
[46] R. Li, Q. Tang, S. Yin, T. Sato, Plasma catalysis for CO_2 decomposition by using different dielectric materials, Fuel Process. Technol. 87 (2006) 617–622, http://dx.doi.org/10.1016/j.fuproc.2006.01.007.
[47] R. Li, Influence of dielectric barrier materials to the behavior of dielectric barrier discharge plasma for CO_2 decomposition, Solid State Ionics 172 (2004) 235–238, http://dx.doi.org/10.1016/j.ssi.2004.02.036.
[48] Q. Yu, M. Kong, T. Liu, J. Fei, X. Zheng, Characteristics of the decomposition of CO_2 in a dielectric packed-bed plasma reactor, Plasma Chem. Plasma Process. 32 (2012) 153–163, http://dx.doi.org/10.1007/s11090-011-9335-y.
[49] X. Duan, Z. Hu, Y. Li, B. Wang, Effect of Dielectric packing materials on the decomposition of carbon dioxide using DBD microplasma reactor, AlChe. 61 (2015) 898–903, http://dx.doi.org/10.1002/aic.
[50] H.H. Kim, A. Ogata, S. Futamura, Oxygen partial pressure-dependent behavior of various catalysts for the total oxidation of VOCs using cycled system of adsorption and oxygen plasma, Appl. Catal. B Environ. 79 (2008) 356–367, http://dx.doi.org/10.1016/j.apcatb.2007.10.038.
[51] T. Nozaki, N. Muto, S. Kado, K. Okazaki, Dissociation of vibrationally excited methane on Ni catalyst, Catal. Today 89 (2004) 57–65, http://dx.doi.org/10.1016/j.cattod.2003.11.040.
[52] X. Tu, H.J. Gallon, J.C. Whitehead, Plasma-assisted reduction of a NiO/Al_2O_3 catalyst in atmospheric pressure H_2/Ar dielectric barrier discharge, Catal. Today 211 (2013) 120–125, http://dx.doi.org/10.1016/j.cattod.2013.03.024.
[53] C.-J. Liu, J. Zou, K. Yu, D. Cheng, Y. Han, J. Zhan, C. Ratanatawanate, B.W.-L. Jang, Plasma application for more environmentally friendly catalyst preparation, Pure Appl. Chem. 78 (2006) 1227–1238, http://dx.doi.org/10.1351/pac200678061227.
[54] H.J. Gallon, X. Tu, M.V. Twigg, J.C. Whitehead, Plasma-assisted methane reduction of a NiO catalyst—low temperature activation of methane and formation of carbon nanofibres, Appl. Catal. B Environ. 106 (2011) 616–620, http://dx.doi.org/10.1016/j.apcatb.2011.06.023.
[55] A.E. Wallis, J.C. Whitehead, K. Zhang, Plasma-assisted catalysis for the destruction of CFC-12 in atmospheric pressure gas streams using TiO_2, Catal. Lett. 113 (2007) 29–33, http://dx.doi.org/10.1007/s10562-006-9000-x.
[56] S. Mahammadunnisa, E.L. Reddy, D. Ray, C. Subrahmanyam, J.C. Whitehead, CO_2 reduction to syngas and carbon nanofibres by plasma-assisted in situ

decomposition of water, Int. J. Greenh. Gas Control. 16 (2013) 361–363, http://dx.doi.org/10.1016/j.ijggc.2013.04.008.
[57] J. Van Durme, J. Dewulf, W. Sysmans, C. Leys, H. Van Langenhove, Efficient toluene abatement in indoor air by a plasma catalytic hybrid system, Appl. Catal. B Environ. 74 (2007) 161–169, http://dx.doi.org/10.1016/j.apcatb.2007.02.006.
[58] H. Wang, J. Li, X. Quan, Y. Wu, Enhanced generation of oxidative species and phenol degradation in a discharge plasma system coupled with TiO_2 photocatalysis, Appl. Catal. B Environ. 83 (2008) 72–77, http://dx.doi.org/10.1016/j.apcatb.2008.02.004.
[59] X. Tu, H.J. Gallon, M.V. Twigg, P.A. Gorry, J.C. Whitehead, Catalyst in a coaxial dielectric barrier discharge reactor, J. Phys. D Appl. Phys. 44 (2011) 274007, http://dx.doi.org/10.1088/0022-3727/44/27/274007.
[60] T. Nozaki, K. Okazaki, Innovative methane conversion technology using atmospheric pressure non-thermal plasma, J. Japan Pet. Inst. 54 (2011) 146–158, http://dx.doi.org/10.1627/jpi.54.146.
[61] Y. Guo, X. Liao, D. Ye, Detection of hydroxyl radical in plasma reaction on toluene removal, J. Environ. Sci. 20 (2008) 1429–1432, http://dx.doi.org/10.1016/S1001-0742(08)62544-9.
[62] X. Bin Liao, Y.F. Guo, J.H. He, W.J. Ou, D.Q. Ye, Hydroxyl radicals formation in dielectric barrier discharge during decomposition of toluene, Plasma Chem. Plasma Process. 30 (2010) 841–853, http://dx.doi.org/10.1007/s11090-010-9253-4.
[63] A. Berthelot, A. Bogaerts, Modeling of plasma-based CO_2 conversion: lumping of the vibrational levels, Plasma Sources Sci. Technol. 25 (2016) 45022, http://dx.doi.org/10.1088/0963-0252/25/4/045022.
[64] R. Snoeckx, S. Heijkers, K. Van Wesenbeeck, S. Lenaerts, A. Bogaerts, CO_2 conversion in a dielectric barrier discharge plasma: N_2 in the mix as a helping hand or problematic impurity?, Energy Environ Sci. 9 (2016) 30–39, http://dx.doi.org/10.1039/C5EE03304G.
[65] F.A.L. Dullien, Porous media – fluid transport and pore, Structure (1991).
[66] S. Mahammadunnisa, P. Manoj Kumar Reddy, E. Linga Reddy, C. Subrahmanyam, Catalytic DBD plasma reactor for CO oxidation by in situ N_2O decomposition, Catal. Today 211 (2013) 53–57, http://dx.doi.org/10.1016/j.cattod.2013.03.028.
[67] A. Jahanmiri, M.R. Rahimpour, M. Mohamadzadeh Shirazi, N. Hooshmand, H. Taghvaei, Naphtha cracking through a pulsed DBD plasma reactor: effect of applied voltage, pulse repetition frequency and electrode material, Chem. Eng. J. 191 (2012) 416–425, http://dx.doi.org/10.1016/j.cej.2012.02.031.
[68] M. Ramakers, I. Michielsen, R. Aerts, V. Meynen, A. Bogaerts, Effect of argon or helium on the CO_2 conversion in a dielectric barrier discharge, Plasma Process. Polym. 12 (2015) 755–763, http://dx.doi.org/10.1002/ppap.201400213.
[69] J. Niu, X. Yang, A. Zhu, L. Shi, Q. Sun, Y. Xu, C. Shi, Plasma-assisted selective catalytic reduction of NOx by C_2H_2 over Co-HZSM-5 catalyst, Catal. Commun. 7 (2006) 297–301, http://dx.doi.org/10.1016/j.catcom.2005.10.016.
[70] S. Kameshima, K. Tamura, Y. Ishibashi, T. Nozaki, Pulsed dry methane reforming in plasma-enhanced catalytic reaction, Catal. Today 256 (2015) 67–75, http://dx.doi.org/10.1016/j.cattod.2015.05.011.
[71] M. Kraus, B. Eliasson, U. Kogelschatz, A. Wokaun, CO_2 reforming of methane by the combination of dielectric-barrier discharges and catalysis, Phys. Chem. Chem. Phys. 3 (2001) 294–300, http://dx.doi.org/10.1039/b007015g.
[72] J. Pype, B. Michielsen, E.M. Seftel, S. Mullens, V. Meynen, Development of alumina microspheres with controlled size and shape by vibrational droplet coagulation, J. Eur. Ceram. Soc. (2016), http://dx.doi.org/10.1016/j.jeurceramsoc.2016.07.020.
[73] C.J. Van Oers, K. Góra-Marek, B. Prelot, J. Datka, V. Meynen, P. Cool, Demonstrating the benefits and pitfalls of various acidity characterization techniques by a case study on bimodal aluminosilicates, Langmuir 30 (2014) 1880–1887, http://dx.doi.org/10.1021/la4034194.
[74] J. Rouquerol, G. Baron, R. Denoyel, H. Giesche, J. Groen, P. Klobes, P. Levitz, A.V. Neimark, S. Rigby, R. Skudas, K. Sing, M. Thommes, K. Unger, Liquid intrusion and alternative methods for the characterization of macroporous materials (IUPAC Technical Report), Pure Appl. Chem. 84 (2012) 107–136, http://dx.doi.org/10.1351/pac-rep-10-11-19.
[75] Q. Wang, B. Yan, Y. Jin, Y. Cheng, Dry reforming of methane in a dielectric barrier discharge reactor with Ni/Al_2O_3 catalyst: interaction of catalyst and plasma, Energy Fuels 23 (2009) 4196–4201, http://dx.doi.org/10.1021/ef900286j.
[76] K. Van Laer, A. Bogaerts, How bead size and dielectric constant affect the plasma behaviour in a packed bed plasma reactor, Plasma Sources Sci. Technol. (2017) (under Rev.).
[77] K. Van Laer, A. Bogaerts, Influence of gap size and dielectric constant of the packing material on the plasma behaviour in a packed bed dbd reactor: a fluid modelling study, Plasma Process. Polym. 14 (2017) e1600129, http://dx.doi.org/10.1002/ppap.201600129.
[78] T.D. Butterworth, The effects of particle size on CO2 reduction in packed bed dielectric barrier discharge plasma reactors (PhD thesis), 2015.
[79] N.P. Bansal, R.H. Doremus, Handbook of Glass Properties, 1986.
[80] T. Tojo, T. Atake, T. Mori, H. Yamamura, Heat capacity and thermodynamic functions of zirconia and yttria-stabilized zirconia, J. Chem. Thermodyn. 31 (1999) 831–845, http://dx.doi.org/10.1006/jcht.1998.0481.
[81] Y. Takahashi, H. Yokokawa, H. Kadokura, Y. Sekine, T. Mukaibo, Laser-flash calorimetry I. Calibration and test on alumina heat capacity, J. Chem. Thermodyn. 11 (1979) 379–394, http://dx.doi.org/10.1016/0021-9614(79)90058-2.
[82] Y. He, Heat capacity, thermal conductivity, and thermal expansion of barium titanate-based ceramics, Thermochim. Acta. 419 (2004) 135–141, http://dx.doi.org/10.1016/j.tca.2004.02.008.
[83] M.W.J. Chase, NIST-JANAF Themochemical Tables, J. Phys. Chem. Ref. Data, 4th ed., 1998.
[84] J.C. Whitehead, Plasma–catalysis: the known knowns, the known unknowns and the unknown unknowns, J. Phys. D. Appl. Phys. 49 (2016) 243001, http://dx.doi.org/10.1088/0022-3727/49/24/243001.
[85] Y.R. Zhang, K. Van Laer, E.C. Neyts, A. Bogaerts, Can plasma be formed in catalyst pores? A modeling investigation, Appl. Catal. B Environ. 185 (2016) 56–67, http://dx.doi.org/10.1016/j.apcatb.2015.12.009.
[86] Y. Zhang, H.-Y. Wang, Y.-R. Zhang, A. Bogaerts, Formation of microdischarges inside a mesoporous catalyst in dielectric barrier discharge plasmas, Plasma Sources Sci. Technol. 26 (2017), http://dx.doi.org/10.1088/1361-6595/aa66be.